

# Longitudinal structures in Mars' upper atmosphere as observed by MAVEN/NGIMS

---

Guiping Liu<sup>1</sup>, Scott England<sup>1,4</sup>, Robert J. Lillis<sup>1</sup>, Paul R. Mahaffy<sup>2</sup>, Meredith Elrod<sup>2</sup>, Mehdi Benna<sup>2</sup>, Bruce Jakosky<sup>3</sup>

## Affiliations

<sup>1</sup>Space Sciences Laboratory, University of California, Berkeley, California, USA, <sup>2</sup>Goddard Space Flight Center, NASA, Greenbelt, Maryland, USA

<sup>3</sup>Laboratory for Atmosphere and Space Physics, University of Colorado Boulder, Boulder, Colorado, USA

<sup>4</sup>Now in Aerospace and Ocean Engineering, Virginia Polytechnical Institute and State University, Blacksburg, Virginia, USA

## Abstract

Here we report the first comprehensive study of longitudinal structures in Mars' neutral upper atmosphere associated with atmospheric tides in composition, density and temperature using the MAVEN/NGIMS observations during 2015. These are *in situ* measurements of number densities of atmospheric species (including CO<sub>2</sub>, Ar, N<sub>2</sub>, and CO) in the altitude range from 120-200 km above the areoid (corresponding to a total density range from  $\sim 10^8$ - $10^{11}$  cm<sup>-3</sup>), providing a dataset that is larger than all previous measurements of these waves combined. These observations span from  $\pm 70^\circ$  latitude, and cover a wide range of local times and solar longitudes (Ls), allowing for the study of longitudinal structures under various conditions. Furthermore, the data in May and November 2015 are at similar latitudes and local times, but different Ls ( $\sim 340^\circ$  in May, close to northern spring equinox, and  $70^\circ$  in November, close to northern summer solstice and aphelion), ideal for studying the seasonal effects of tides. Our analysis shows that in each month the Ar density varies with longitude having a large wave structure. It is dominated by wave-2 and 3, accounting for 8-16% of the change of the mean density. Comparison shows that the longitudinal structures at a constant CO<sub>2</sub> density level have different amplitudes at different seasons, although their patterns are similar. The temperature structure has a phase difference from the density variation, indicating the

This article has been accepted for publication and undergone full peer review but has not been through the copyediting, typesetting, pagination and proofreading process which may lead to differences between this version and the Version of Record. Please cite this article as doi: 10.1002/2016JA023455

dissipation of tides in this altitude region. The longitudinal structure is seen in all species, including major and minor species, consistent with the tidal signatures.

## 1 Introduction

Atmospheric tides, originating from the interaction of solar radiation with Mars' topography and the atmosphere, can create significant changes in the upper atmosphere density and dynamics [e.g. *Keating et al.*, 1998; *Forbes and Hagan*, 2000; *Forbes et al.*, 2002; *Wilson* 2002; *Bougher et al.*, 2004; *Moudden and Forbes*, 2008, 2014; *Withers et al.*, 2011; *England et al.*, 2016]. Tides are planetary-scale oscillations with periods that are harmonics of the solar day. By convention they are represented as:

$$A_{n,s} \cos(n\Omega t + s\lambda - \phi_{n,s}) \quad (1)$$

where  $t$  is time in sols,  $\lambda$  is east longitude,  $n$  is the harmonic ( $n = 1$  for diurnal tide,  $n = 2$  for semidiurnal tide, ...),  $\Omega = 2\pi \text{ sol}^{-1}$  is the planetary rotation rate in radians per second,  $s$  is the zonal wave number ( $s = \dots -2, -1, 0, 1, 2, \dots$ , where  $s > 0$  implies the westward propagation,  $s < 0$  implies the eastward propagation, and  $s = 0$  represents the standing oscillation),  $A_{n,s}$  is the amplitude, and  $\phi_{n,s}$  is the phase, and both  $A_{n,s}$  and  $\phi_{n,s}$  are functions of height and latitude [e.g. *Forbes and Hagan*, 2000].

Rewriting in terms of local time ( $t_{LT}$ ), equation (1) becomes

$$A_{n,s} \cos(n\Omega t_{LT} + (s - n)\lambda - \phi_{n,s}) \quad (2)$$

In the fixed local time reference frame, tides appear to have zonal wavenumbers given by  $|s - n|$  [e.g. *Forbes et al.*, 2002]. Components with  $s = n$  are longitude independent (zonally symmetric), and they have the zonal phase speed equal to  $-\Omega$ . That is they propagate westward at the same speed as the apparent motion or migration of the Sun when observed from the planet. These Sun-synchronous tides are referred to as “migrating” tides. The  $s \neq n$  longitude-dependent (zonally asymmetric) components are called “nonmigrating” tides. Observed by a ground-based observer, the nonmigrating tides can travel opposite to the Sun's apparent motion or travel faster than the Sun in the same direction.

The westward or eastward propagating diurnal tides are commonly denoted by DWs or DEs, where  $s$  is the absolute zonal wave number. For semidiurnal tides, “S” replaces “D”. The standing oscillations are denoted by D0 and S0. For example, DE2 denotes a diurnal tide propagating eastward with wavenumber 2. In the fixed local time reference frame, DE2 tide would produce a longitudinal wavenumber-3 structure ( $n = 1$ ,  $s = -2$ , and  $|s - n| = 3$ ).

Longitudinal wave 2 and 3 structures in Mars' thermosphere have been frequently seen in fixed local time observations of atmospheric pressure, density and temperature [e.g. *Keating*

*et al.*, 1998; *Hinson et al.*, 1999; *Bougher et al.*, 2001; *Wilson* 2002; *Tolson et al.*, 2005, 2008; *Seth et al.*, 2006; *Withers et al.*, 2006, 2011; *England et al.*, 2016]. Due to their long vertical wavelengths, it is believed that these are the signatures of the DE1 and DE2 tides, which may propagate upward through the atmosphere without significant dissipation and thus efficiently contribute to large-scale variations at thermospheric heights [e.g. *Forbes and Hagan*, 2000; *Wilson*, 2002].

Modeling studies [e.g. *Hollingsworth and Barnes*, 1996; *Forbes and Hagan*, 2000; *Forbes et al.*, 2002; *Wilson* 2002; *Bougher et al.*, 2004; *Angelats i Coll et al.*, 2004; *Moudden and Forbes*, 2008, 2014] have demonstrated that DE1, DE2, and DE3 tides are most important in driving the longitudinal wave 2-4 patterns although semidiurnal tides may also be responsible. It is generally believed that stationary planetary waves forced by the topography are unable to directly propagate to thermospheric heights [e.g. *Wilson* 2002]. However, by interacting with the diurnal tides the topographic signature may be carried into the thermosphere [e.g. *Withers et al.* 2011; *Medvedev et al.*, 2016]. Through different mechanisms, the upper atmosphere longitudinal structures could respond to both diurnal tides and stationary planetary waves that propagate up from the lower atmosphere.

Accelerometer measurements of atmospheric densities have revealed large variations with density amplitudes of ~20% in the aerobraking region (90-150 km) as obtained from the Mars Global Surveyor (MGS), Mars Odyssey, and Mars Reconnaissance Orbiter missions [e.g. *Keating et al.*, 1998; *Wilson* 2002; *Withers et al.*, 2003; *Tolson et al.*, 2007]. Due to Mars' topography, these variations are much larger than the thermospheric density perturbations on Earth peaking at values around only 5% [e.g. *Oberheride and Forbes*, 2008]. Observations of atmospheric tidal effects on Mars' upper atmosphere have also been made using techniques including atmospheric refractivity of radio waves [*Bougher et al.*, 2004; *Cahoy et al.*, 2006], atmospheric absorption of stellar ultraviolet light [*Forget et al.*, 2009; *Withers et al.*, 2011], and multichannel observations of infrared emissions [*Lee et al.*, 2009]. The impact of such waves on atmospheric composition is expected to be significant, but has only been recently observed by Mars Atmosphere and Volatile Evolution Mission (MAVEN) [*Jakosky et al.*, 2015] as reported by *England et al.* [2016].

*Lo et al.* [2015] presented the first observations of atmospheric tides made by MAVEN/IUVS using the remote sensing observations of the CO<sub>2</sub><sup>+</sup> UV Doublet airglow emission during October 2014, shortly after the spacecraft reached Mars. By combining *in situ* and remote observations, *England et al.* [2016] identified the signatures of non-migrating tides in several atmospheric species. However, these studies are for only one local time and a

limited range of latitudes ( $0^{\circ}$ - $30^{\circ}$ N), so the behavior of tides at different local times and latitudes has not been studied using MAVEN observations. In addition, *Moudden and Forbes* [2014] have found that, at 60-80 km, above the areoid the DE2 activity peaks during the northern summer season and diminishes before the northern autumn equinox. Longitudinal wave structures have also been observed in the altitude region 70-120 km, and they appear to change with season [e.g. *Withers et al.*, 2011]. However, this change may be due to the local time and latitude variations as these observations between different seasons are for different local times and latitudes. The seasonal effect of tides is expected to be observable in the thermosphere region, but has yet to be identified from MAVEN data that allow for the separation of seasonal change from latitude and local time.

The Neutral Gas Ion Mass Spectrometer (NGIMS) [*Mahaffy et al.*, 2014] onboard the MAVEN spacecraft has made *in situ* measurements of atmospheric densities for several species (primarily CO<sub>2</sub>, Ar, N<sub>2</sub>, and CO) in the altitude range from 120-200 km above the areoid in the upper atmosphere. The observations from February-December 2015 are available over a broad range of latitudes and local times. Furthermore, the data in May and November are at similar latitudes and local times but different solar longitudes ( $\sim 340^{\circ}$  in May, close to northern spring equinox, and  $70^{\circ}$  in November, close to northern summer solstice and aphelion). These provide a dataset that is larger than all previous measurements of tidal waves combined and allow for the study of density changes under various conditions. Here we report the first comprehensive study of atmospheric tides in Mars' upper atmosphere using these many months of MAVEN/NGIMS observations.

## 2 NGIMS DATA

The NGIMS data are available in 2015 from February-December. As listed in Table 1, the available Level 2 (version 6, revision 1) data are almost continuous, except for a few gaps on February 18-20, April 4-14, May 27-July 1, and August 12-20. The instrument operated in a different mode before February, and so these months are not included. Data from early 2016 are available, but these are nighttime observations and for northern high latitudes, where tides signatures are less clear, and as such are not included in our analysis.

Month	Dates Available	Number of Orbits
Feb	11-17 (has dip deep); 21-28	74
Mar	1-31	139
Apr	1-3; 15-30 (has deep dip)	82

May	1-26	117
July	2-31 (has deep dip)	152
August	1-11; 21-31	95
September	2-30 (has deep dip)	127
October	1-31	153
November	1-30	146
December	1-31 (has deep dip)	145

Table 1: Available NGIMS Level 2 v6 r1 data in each month of 2015. Note: observations below 150 km altitude (above the areoid) are available during “deep dip” experiments in February, April, July, September and December.

NGIMS is a quadrupole mass spectrometer, designed to measure atmospheric densities at altitudes below 500 km above the areoid. We have limited our analysis to below 200 km altitude given that at higher altitudes the densities decrease and the tides signatures are less clear, especially in the minor species. The spacecraft is in an eccentric 4.5 hour orbit, with apoapsis around 6220 km and periapsis around 150 km [Jakosky *et al.*, 2015]. The periapsis altitude changes over time in response to the changing atmospheric density and small “orbital trim” thruster-firing maneuvers [Jakosky *et al.*, 2015]. Further five “deep dip” experiments have been carried during February, April, July, September and November of 2015. Each experiment lasted for ~7 consecutive days, when periapsis approaches altitudes as low as 120 km (see Figure 1). These experiments allow for measurements of the homopause (i.e. the altitude below which turbulent mixing results in a single scale height for all species), and are useful for profiling the entire upper atmosphere down to where it connects to the lower atmosphere [Jakosky *et al.*, 2015]. We have included these profiles but only for higher altitudes (>150 km) since these experiments occur only at limited times. Observations are made 4-5 orbits per day, and in total there are more than 1200 orbits throughout 2015.

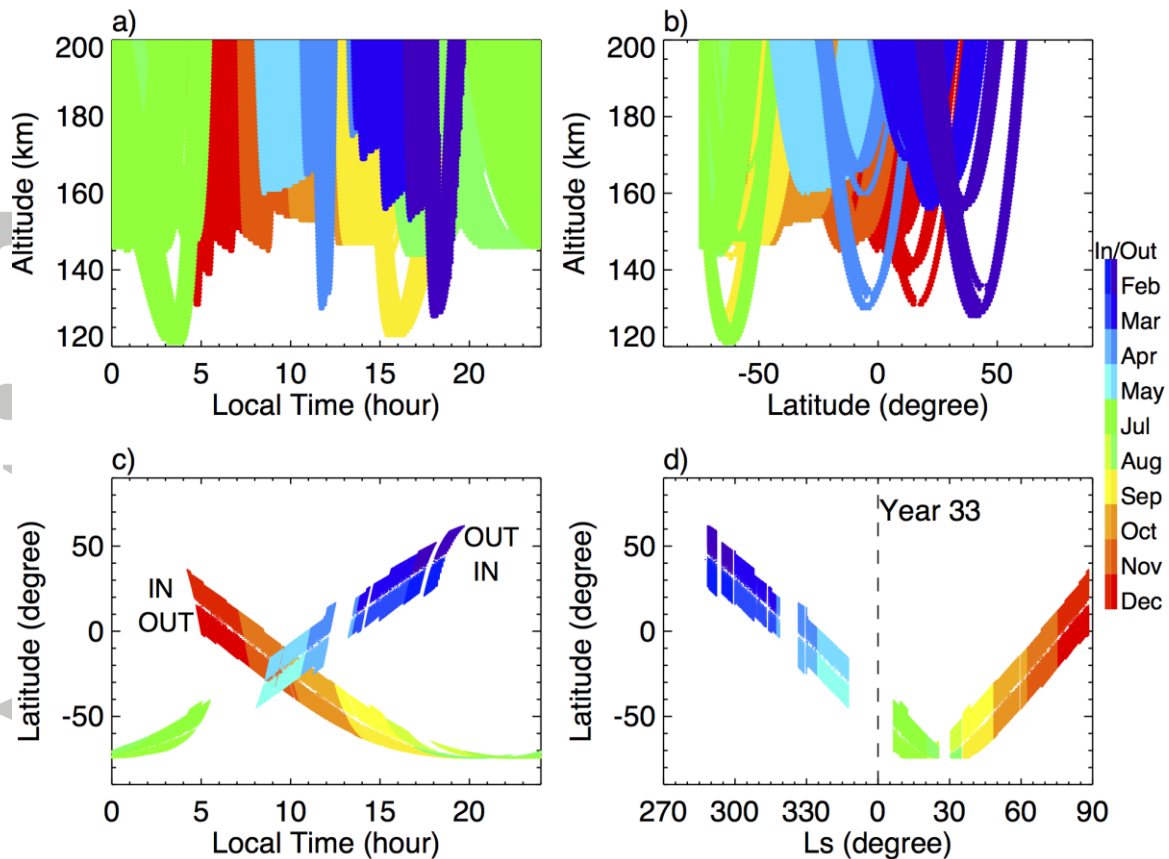


Figure 1: Distributions of the NGIMS data below 200 km altitude (above the areoid) for each month of 2015. Different colors are for different months, and the relatively lighter/darker colors (in c and d) are for inbound/outbound observations, respectively. The data are presented versus in a) local time and altitude, b) latitude and altitude, c) local time and latitude, and d) solar longitude (Ls) and latitude. In d), the dashed line marks the beginning of Martian year 33.

Figure 1 shows the coverage of the NGIMS data (from periapsis-200 km altitude for each orbit in each month) during 2015. Each orbit below 200 km altitude lasts for ~600 seconds, so the region measured during one orbit pass is large for ~20° latitude. The data span from ±70° latitude, and cover a wide range of local times and Ls. Specifically, the data from May and November are for similar latitudes and local times, but different Ls (~340° in May, close to northern spring equinox, and 70° in November, close to northern summer solstice and aphelion).

For each month, the data provide complete longitudinal coverage (plots are not included) as the planet rotates below MAVEN's orbit. They are over limited latitudes and local times (usually within 30° latitude and 3 hour range) due to the slow precession of the orbit. Tides are planetary-scale signatures, and the prominent components present in the thermosphere are

believed to have periods of 24 hours. In addition, tides have been observed to evolve in timescales of several weeks to months [e.g. *Mazarico et al.*, 2008; *Withers et al.*, 2003]. It is thus reasonable to assume that the tidal signatures are the same over the time interval of one month.

Given that the data are missing from April 4-14, there are insufficient data to perform an analysis with the April data alone. Thus, we have combined the first 3 days in April with March. Data in July and August are for high latitude ( $\sim 50^{\circ}$ - $70^{\circ}$ S) and nighttime ( $\sim 17$ - $05$  hr local time) observations. As the Ar density decreases greatly at night, the tidal signatures are not so clear in July and August. We have thus excluded these two months. In total, we have grouped 7 months of data to study the longitudinal structures and atmospheric tides. The NGIMS observations are at high altitude resolution ( $\sim 1$  km within this range). To determine the longitudinal structures, we have interpolated the data into regular grids at 1km altitude steps, and binned the data into  $30^{\circ}$  longitude intervals for each group.

NGIMS has both open and closed source modes, which enable it to measure both non-reactive and reactive atmospheric species. The measurements relevant are those of  $\text{CO}_2$ , Ar,  $\text{N}_2$  and CO, comprising all of the major constituents of Mars' upper atmosphere. While the closed source is used to measure non-reactive species ( $\text{CO}_2$ , Ar, and  $\text{N}_2$ ) on every orbit, the open source measures both reactive and non-reactive species (CO) on alternate orbits.

For each orbit, NGIMS repeatedly samples one species throughout all altitudes. This provides a series of density measurements (i.e. altitude profile of density), allowing for derivations of atmospheric temperatures. Following the method described by *Snowden et al.* [2013], we have calculated atmospheric pressures at all altitudes assuming hydrostatic equilibrium, and converted these to temperatures using the ideal gas law. The pressures are calculated by integrating the densities along the orbit from the top boundary of the atmosphere (250 km altitude is used in this study) down to periapsis. As described [e.g. *Korablev et al.*, 2001; *Forget et al.*, 2009], this calculation relies on the assumption that the density changes solely with altitude. The assumption becomes invalid in region close to periapsis, where the spacecraft is moving essentially horizontally, and small-scale wave structures are present, which do not represent changes with altitude [e.g. *Yigit et al.*, 2015]. Therefore, we have limited our temperature calculations to altitudes at least 5 km above periapsis, and we have only used the inbound portions of orbits. Furthermore, the calculations are not reliable where the densities are low, especially on the nightside, so the temperatures are not derived for all measurements.

### 3 Longitudinal Structures

Longitudinal structures in each group (month) are presented for Ar in the following section. In section 3.2, the structures seen in different species will be presented, and the differences between seasons will be compared.

#### 3.1 Ar Density Variations

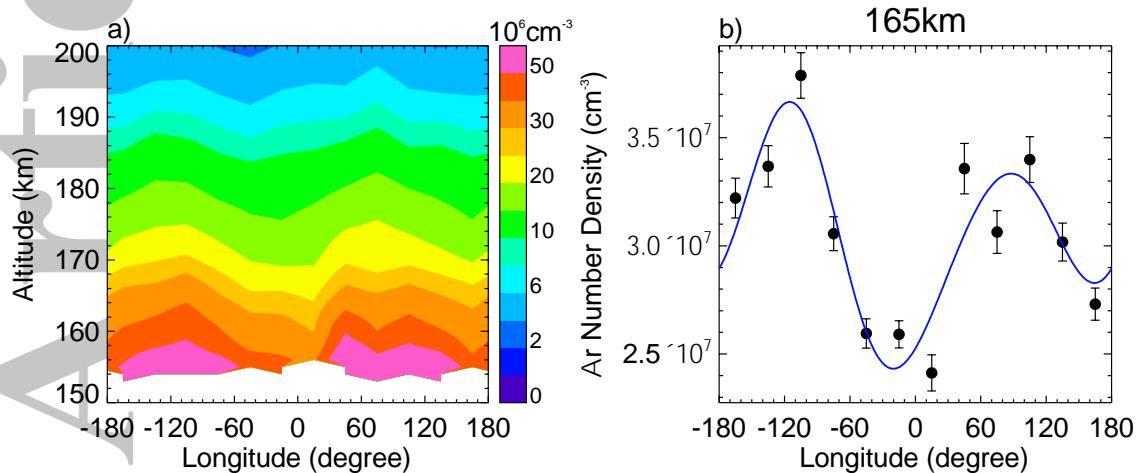


Figure 2: a) Averaged Ar densities in March 2015 presented versus longitude and altitude. b) Least-squares fits (blue curve) of the data at 165 km altitude to the longitudinal wave structures including wavenumbers 0-3. Black circles denote the mean densities at each longitude bin, and the error bars represent the standard deviations of the data in each bin. A strong wave-2 structure is seen for this month.

Figure 2a presents the mean observed Ar densities using both inbound and outbound observations for March 2015, presented versus longitude and altitude. A clear longitudinal wave structure is seen, and this signature is the largest at the lowest altitudes  $\sim 155$  km. To determine the structure, we have fitted the data to harmonics with the wavenumbers from 0-3 using least-squares fits. As an example, Figure 2b shows the fitting at a given altitude of 165 km. The reconstruction based on the least-squares fits indicates the presence of the wave-2 structure at this altitude. This structure dominates the longitudinal density variation, but the asymmetry suggests that other wavenumbers are also present.

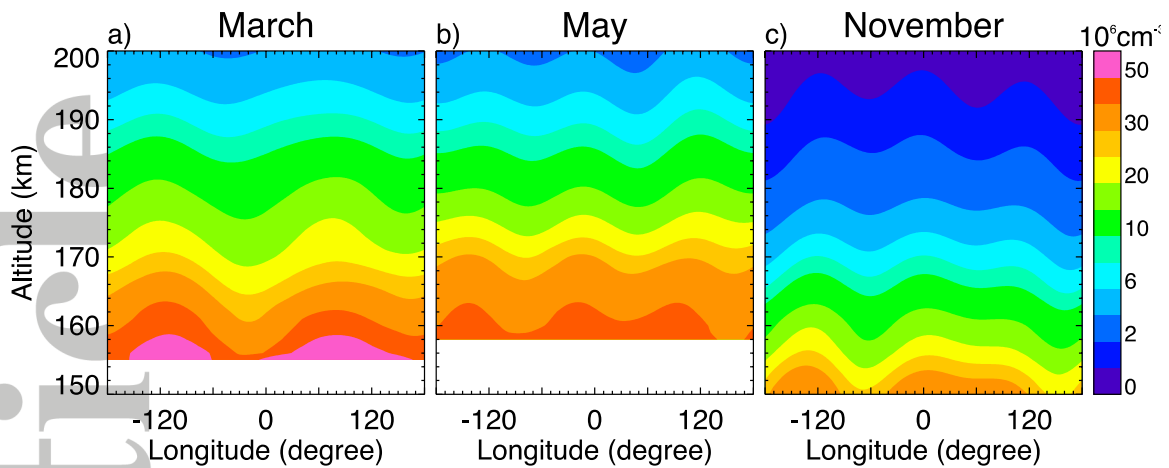


Figure 3: Reconstructions of least-squares fits of Ar densities to the longitudinal wave structures including wavenumbers 0-3 for a): March, b): May and c): November of 2015.

The least-squares fits have been repeated for each 1 km altitude from ~150-200 km, and the reconstructions are shown in Figure 3a. The wave-2 structure occurs throughout almost all altitudes. This structure is the largest at the lowest altitude, and its amplitude decreases with increasing altitude. The same wave structure has been presented and discussed by *England et al.* [2016], in which these were seen in both the NGMIS and limb-viewing IUVS [e.g. *McClintock et al.*, 2014] observations and between multiple species. Here this analysis is for the similar set of data (over similar time interval, latitude and local time), which implies that this wave structure is associated with atmospheric non-migrating tides.

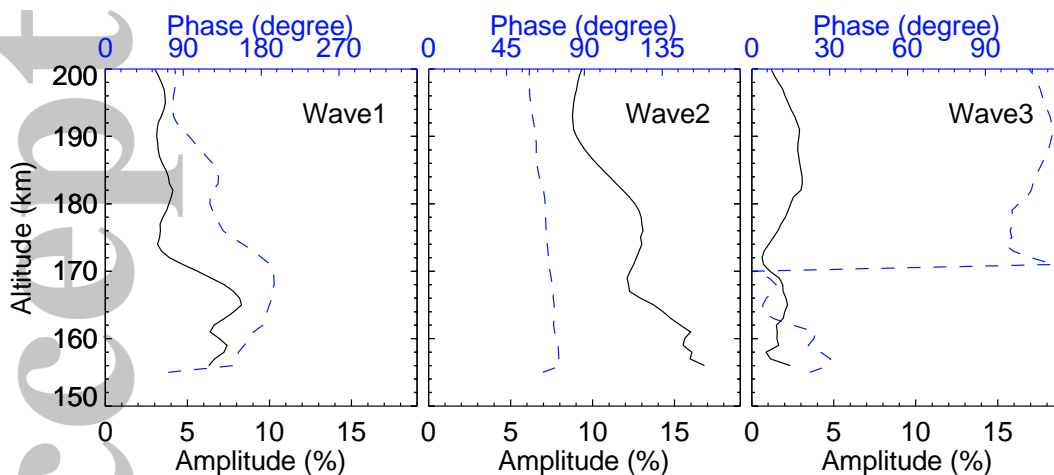


Figure 4: Amplitudes (black solid curves) and phases (blue dashed curves) of wave 1-3 structures at each altitude as seen in Ar density in March.

Figure 4 shows again the dominance of wave 2, with an amplitude ranging from ~15% of the zonal mean density at the lowest altitudes to ~10% at higher altitudes. Wave 1 and 3 are

also present, but have smaller amplitudes at all altitudes. Below 170 km altitude, the wave-1 amplitudes approach the largest values of ~7%, but they are 2-3 times smaller than the wave-2 amplitudes. The amplitude of wave 3 is the smallest at only 2-3% of the mean density. The phase coherence (almost constant) between different altitudes, specifically for wave-2, shows that our wave fits are reliable.

*Withers et al.* [2011] have found that both wave-2 and wave-3 can dominate the longitudinal structures at 70-120 km altitudes, and the wave amplitudes change dramatically with altitude. Our observations are for higher altitudes, but similar features are seen. This shows that tides are responsible for the observed wave components at all altitudes.

The data in May and November are at similar latitudes and local times but different solar longitudes (~340° in May, close to northern spring equinox, and 70° in November, close to northern summer solstice and aphelion). Figures 3b and 3c present the Ar density variations in May and November 2015. The wave 2 signature is still present, being larger in November at lower altitudes ~160 km. However, the wave 3 becomes stronger above 165 km altitude. Compared to Figure 3a, this shows different features in November when the mean density is much lower and may reflect a seasonally-dependent process. However, the local time and latitude differences should also be considered.

Group	Month	Latitude (degree)	Local Time (hour)	Ls (degree)	Altitude (km)	Mean ( $10^7 \text{cm}^{-3}$ )	Wave 1		Wave 2		Wave 3	
							Amplitude (%)	Phase (degree)	Amplitude (%)	Phase (degree)	Amplitude (%)	Phase (degree)
1	Feb	38	18	290	164	1.8	6	187	<b>12</b>	67	4	39
2	Mar	22	15	310	174	1.8	3	159	<b>13</b>	68	1	97
3	May	-21	10	340	172	2.4	3	172	4	172	<b>8</b>	104
4	Sep	-57	15	40	157	2.3	6	28	4	106	<b>8</b>	96
5	Oct	-37	12	55	158	2.7	<b>11</b>	264	6	57	8	100
6	Nov	-13	8	70	154	2.5	6	359	<b>16</b>	41	11	107
7	Dec	9	6	85	148	1.9	8	245	<b>10</b>	58	9	94

Table 2: Amplitudes of wave 1-3 structures in Ar density at the constant CO<sub>2</sub> density level of ~10<sup>9</sup>/cm<sup>3</sup> for each month of 2015 (corresponding altitude levels are given). The dominant wavenumber in each month is marked in bold. The wave phase, zonal mean densities, Ls, local time, and latitude are also listed. Phase is measured in longitude, where east is positive.

Table 2 lists the amplitudes of wave 1-3 structures in Ar density in different months. Here we have selected for fixed altitude levels corresponding to a constant CO<sub>2</sub> density. For the

given CO<sub>2</sub> density of 10<sup>9</sup>/cm<sup>3</sup>, the altitude is at ~174 km and 172 km in March and May (latitude=22°N and 21°S, LT=15 and 10 hour, and Ls=310° and 340°), and the level is at ~154 km in November (latitude=13°S, LT=8 hour, and Ls=70°). Ar densities at these constant altitudes are used to determine the wave structures. As CO<sub>2</sub> and Ar have similar masses and scale heights, the zonal mean Ar densities are similar between different months. This means that the wave amplitudes can be compared directly to each other. It can be seen that there is a large wave signature, dominated by wave 2 and 3, accounting for 8-16% of the mean density change. The wave-2 signature is the largest in November, and the smallest wave is observed in March and May (wave-3 is the smallest in March at ~1%, and the smallest wave in May is wave-1 having an amplitude of ~3%). All three occur at low latitudes and during daytime, but at different Ls. These suggest again that there could be a seasonal effect on the tidal variation.

### 3.2 Seasonal effects and variations between species

Figure 5 provides the comparison of the longitudinal wave structures in density between May and November, and between temperature and density during November. Both Ar densities and temperatures only from the inbound orbit observations are presented. Temperatures are presented for November given that the calculations are more accurate and the tidal signatures are clearer. It can be seen that the density structures (shown in black color) between the two seasons are quite similar, both having a large wave-3 signature. In November, other wavenumbers such as wave-2 are large. Comparing the density with temperature, their variation patterns are very similar but appear to be out of phase, specifically for wave-2 and wave-3 components. This indicates that the temperature variation is due to the adiabatic cooling/warming caused by tides as discussed by *Withers et al.*, [2011].

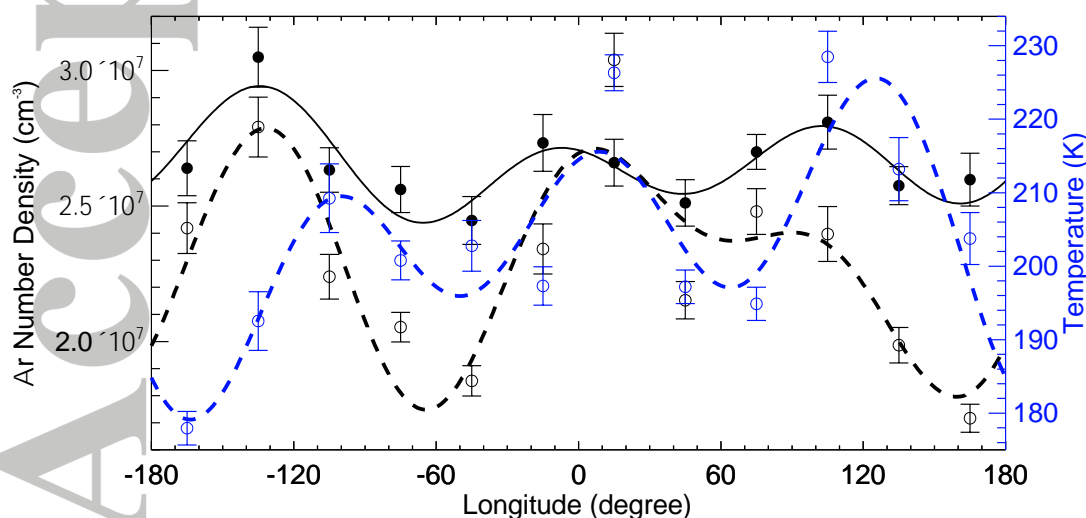


Figure 5: Longitudinal structures in Ar density (black color) and temperature (blue color) for May (solid curve) and November (dashed curves) at the constant CO<sub>2</sub> density level equal to  $\sim 10^9/\text{cm}^3$  ( $\sim 172$  km altitude in May and  $\sim 154$  km in November). Circles (filled symbols are for May and open symbols are for November) denote the mean values at each longitude bin, and the error bars represent the standard deviations of the data.

Figure 6 quantifies the seasonal effects between May and November for wave 1-3. Here both Ar density and temperature are included and only inbound observations are used. It is clear that the density variations from different wavenumbers are different from these two seasons. In May, the wave-3 is the largest, contributing to 5-12% of the mean density change, and the change by wave 1 or 2 is much less at no more than 6%. For November, the changes by the 3 wavenumbers are all larger, ranging from 5-20%.

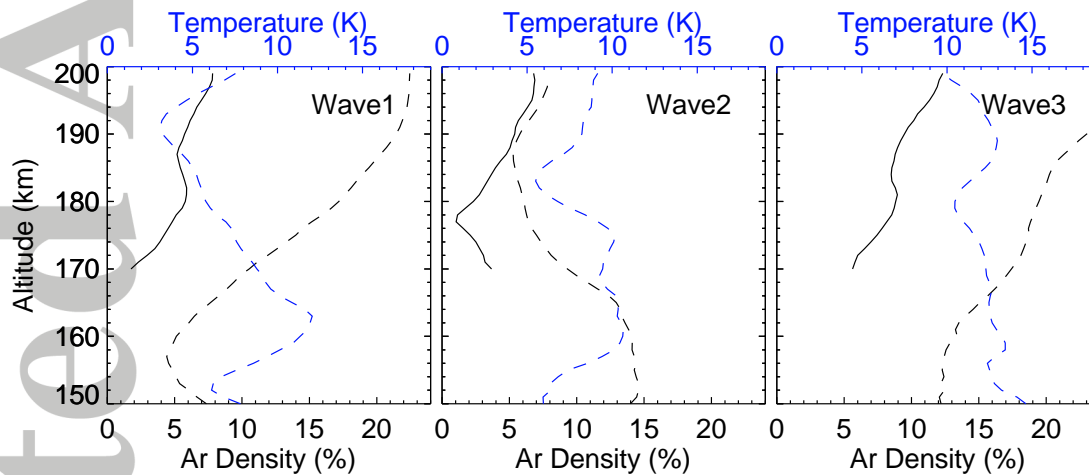


Figure 6: Amplitudes of wave 1-3 structures in Ar density (black color) and temperature (blue color) for May (solid curves) and November (dashed curves), presented versus altitude.

Figure 6 also shows that the temperature variation is  $\sim 10$  K between 155-180 km altitude given that temperatures are only reliable in this altitude range over a more narrow range than density (discussed in Section 2). This temperature variation has a phase difference from the density at a fixed altitude (shown in Figure 5), and this figure (Figure 6) shows the amplitude of the density wave changes with altitude. As explained by *Withers et al.* [2011], these are consistent with the signatures of dissipating tidal waves in this altitude region.

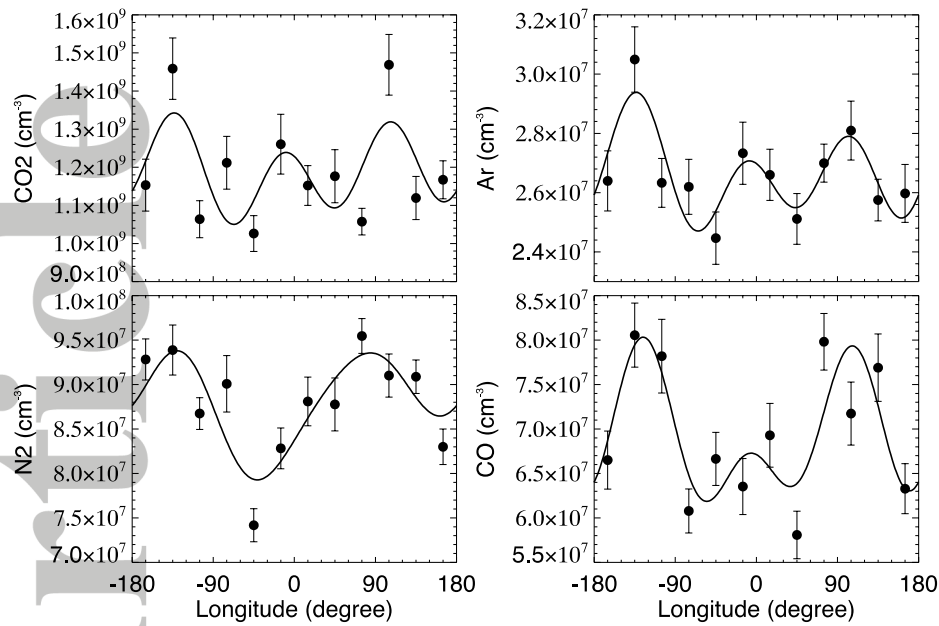


Figure 7: Longitudinal variations in various species at ~172 km altitude ( $\text{CO}_2$  density level equals to  $\sim 10^9/\text{cm}^3$ ) in May.

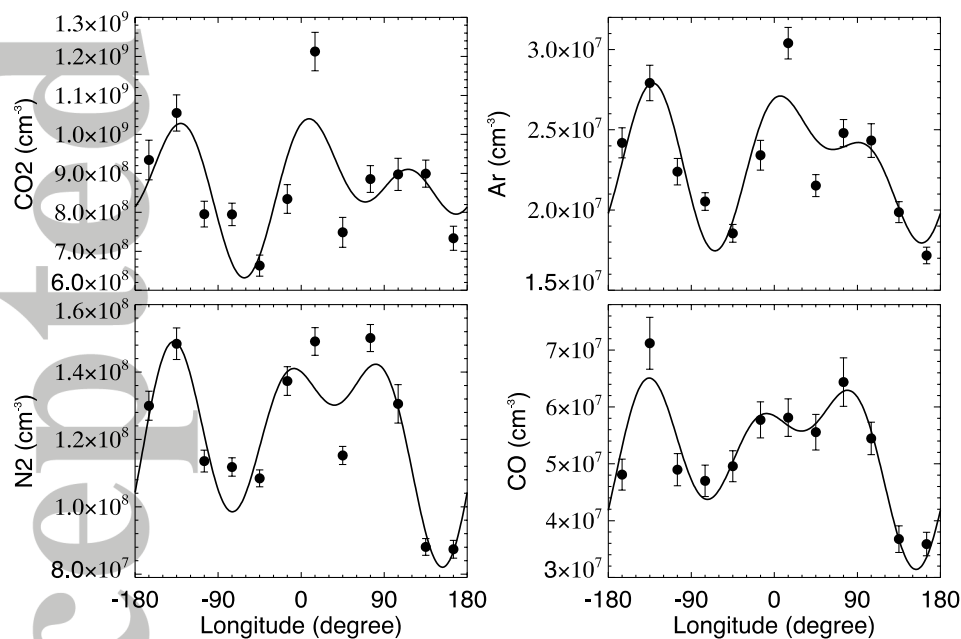


Figure 8: Same as Figure 7 but for November at ~154 km altitude ( $\text{CO}_2$  density level equals to  $\sim 10^9/\text{cm}^3$ ).

Figures 7 and 8 present the longitudinal variations in species of  $\text{CO}_2$ , Ar,  $\text{N}_2$ , and CO for May and November. For comparison, only inbound observations are used for all species (the CO density has large uncertainty in outbound because gases from periapsis tend to build up in the instrument resulting in much higher backgrounds for outbound passes). Here we have

selected for the altitudes corresponding to a constant CO<sub>2</sub> density, so the variation amplitudes can be compared between each other.

	CO <sub>2</sub>			Ar			N <sub>2</sub>			CO		
	W1	W2	W3	W1	W2	W3	W1	W2	W3	W1	W2	W3
May	3	3	<b>9</b>	2	4	<b>6</b>	5	<b>6</b>	1	6	6	<b>9</b>
Nov	4	12	<b>13</b>	5	<b>14</b>	12	9	14	<b>15</b>	10	<b>18</b>	15

Table 3: Amplitudes (%) of longitudinal wavenumber 1-3 (W1, W2 and W3) structures in number densities of various species for May at ~172 km altitude and November at ~154 km altitude, corresponding to the constant CO<sub>2</sub> density level of ~10<sup>9</sup>/cm<sup>3</sup>. The largest component in each species is highlighted in bold. Note: Only inbound observations are used.

As seen in Figures 7 and 8, each species exhibits a large wave signature in the longitudinal variation. Table 3 lists the relative amplitudes of wave 1-3 for all species in both months. It can be seen that wave-3 dominates the variation in the major species of CO<sub>2</sub>, accounting for 9% and 13% of the mean density change in May and November, respectively. For Ar, this wave-3 perturbation is also strong, contributing to 6% and 12% of the changes for these two seasons, but the wave-2 variation is slightly larger in November at 14%. Similarly, CO has the largest perturbation of wave-3 at 9% in May, and the wave-2 variation of 18% is the largest in November. For N<sub>2</sub>, the variation is dominated by wave-2 at 6% in May and wave-3 at 15% in November. Comparing these seasons, all species have a larger wave variation in November than in May, indicating the seasonal effects on the upper atmosphere composition and structure.

Many modeling studies have simulated DE1 and DE2 tides and revealed their importance in controlling the longitudinal structures in the thermosphere [e.g. *Bougher et al.*, 2004; *Angelats i Coll et al.* 2004; *Wilson et al.*, 2002; *Forbes and Miyahara*, 2006; *Moudden and Forbes*, 2008, 2014; *Medvedev et al.*, 2016]. Some of these studies have found that the density amplitudes caused by these tides are ~20% at Ls=30-90° in the tropics [*Bougher et al.*, 2004; *Angelats i Coll et al.* 2004; *Forbes and Miyahara*, 2006]. Using a general circulation model, *Moudden and Forbes* [2014] compared the DE2 amplitudes between Ls=90° and Ls=270°. They found that the tidal amplitudes change with season and the amplitude is larger in northern summer than in northern winter. Our analysis results of the wave amplitudes observed are overall consistent with previous modeling studies for similar conditions.

The relative density variation seen in each of these species is different (the largest wave amplitudes in May are ~9%, 6%, 6% and 9% for CO<sub>2</sub>, Ar, N<sub>2</sub> and CO; the amplitudes in

November are ~13%, 14%, 15% and 18% for these species), which would cause a local change in composition. This is consistent with vertical advection produced by atmospheric tides. These tides have long vertical wavelengths (as indicated by Figure 6), so vertical advection is important (it is more important than eddy diffusion). Vertical advection thus dominates the transport and affects the distributions of atmospheric species. Given that vertical advection is proportional to  $1/\text{scale height}$  [e.g. *Dudis and Reber, 1976*] and different species have different scale heights at thermospheric altitudes, the relative density change in each of the species is expected to be different. *England et al. [2016]* has compared the wave-2 variations of five species in relation to their scale heights. They have found that the relative density change of each species is proportional to  $1/\text{scale height}$ , showing the compositional change caused by tides. Here in this study, it is unclear why in May  $\text{N}_2$  has a large wave-2 variation, but it is larger in  $\text{CO}_2$ . Our analysis result is generally consistent with the signatures being associated with the tides.

The compositional changes are different between the two seasons. Both the density and compositional changes are related to the vertical advection, so they should be proportional to each other. In May, the largest wave perturbations are ~9% in  $\text{CO}_2$  and CO and 6% in Ar and  $\text{N}_2$ , having a compositional difference of ~3%. The perturbations in November are larger in all species (~13% in  $\text{CO}_2$ , 14% in Ar, 15% in  $\text{N}_2$  and 18% in CO), and the compositional difference is as large as ~5%. These variations are associated with tides, and they could also relate to other processes such as the photochemistry. However, identifying these processes requires more than the NGIMS density observations alone. A full explanation of the variations requires a further study that at least includes a photochemical model. Our analysis and the observations presented here can provide inputs to such a study.

## 4 Conclusions

Using atmospheric density measurements from the Neutral Gas Ion Mass Spectrometer (NGIMS) on the Mars Atmosphere Volatile Evolution (MAVEN) mission, we have performed the first comprehensive study of large-scale longitudinal variations associated with atmospheric tides in Mars' neutral upper atmosphere in composition, density and temperature. Many months of *in situ* measurements of number densities of various atmospheric species (including  $\text{CO}_2$ , Ar,  $\text{N}_2$  and CO) in the altitude range from 120-200 km above the areoid are analyzed. These observations are available from February-December 2015, span  $\pm 70^\circ$  latitudes and cover a wide range of local times and solar longitudes (Ls), providing a dataset that is larger than all previous measurements of tides combined.

Furthermore, the observations for May and November are at similar latitudes and local times, but different  $L_s$  ( $\sim 340^\circ$  in May, close to northern spring equinox, and  $70^\circ$  in November, close to northern summer solstice and aphelion), ideal for the study of seasonal changes. The main analysis results are summarized as follows:

1. The Ar observations in each month reveal a large longitudinal structure with dominant wave 2 and 3 wavenumbers in a fixed local time frame. These wave amplitudes vary with altitude, and also depend on latitude, local time and  $L_s$ . The largest wave amplitude is calculated to be equal to 8-16% of the mean density.
2. Comparison of the May and November data shows that the longitudinal structures at a constant  $\text{CO}_2$  density level have different amplitudes between different seasons, although their patterns are similar. This is the first time that we are able to separate the seasonal effect of tides in the thermosphere from the local time and latitude variations.
3. A similar longitudinal wave structure is seen in temperature but has a phase difference from the density variation. Combined with the altitude change of the wave amplitude, these indicate that the temperature variation is the result of the adiabatic cooling/warming due to tides and that these tides dissipate in the thermosphere region.
4. Observations of  $\text{CO}_2$ , Ar,  $\text{N}_2$ , and CO show that the longitudinal wave-2 and wave-3 structures are seen in all species, including major and minor species. These reveal the tidal impact on thermospheric composition. All species have a larger wave variation in November than in May, showing again the seasonal effects of tides.
5. The difference in the relative density perturbation seen in each of these atmospheric species is consistent with vertical advection caused by atmospheric tides. However, it is unclear why  $\text{N}_2$  has a large wave-2 structure in May, but this is much larger in  $\text{CO}_2$ .

### **Acknowledgements**

The NGIMS Level 2 data are publicly available on the Planetary Data System (PDS) at <http://pds.nasa.gov>. G.L., S.L.E., and R.J. Lillis were supported by the NASA Mars Data Analysis Program through grant NNX16AJ42G. The MAVEN mission has been funded through the NASA Mars Exploration Program.

### **References**

Angelats i Coll, M.F. Forget, M.A. López-Valverde, P.L. Read, and S.R. Lewis (2004), Upper atmosphere of Mars up to 120 km: Mars Global Surveyor accelerometer data

- analysis with the LMD general circulation model, *J. Geophys. Res.*, *109*, E01011, doi:10.1029/2003JE002163.
- Bougher, S.W., S. Engel, D.P. Hinson, and J.M. Forbes (2001), Mars Global Surveyor radio science electron density profiles and implications for the neutral atmosphere, *Geophys. Res. Lett.*, *28*, 3091-3094.
- Bougher, S.W., S. Engel, D.P. Hinson, and J.R. Murphy (2004), MGS Radio Science electron density profiles: Interannual variability and implications for the Martian neutral atmosphere, *J. Geophys. Res.*, *109*, E03010, doi:10.1029/2003JE002154.
- Cahoy, K.L., D.P. Hinson, and G.L. Tyler (2006), Radio science measurements of atmospheric refractivity with Mars Global Surveyor, *J. Geophys. Res.*, *111*, E05003, doi:10.1029/2005JE002634.
- Chapman, S., and R.S. Lindzen (1970), *Atmospheric Tides*, 201 pp., D. Reidel, Norwell, MA.
- Dudis, J.J., and C.A. Reber (1976), Compositional effects in thermospheric gravity waves, *Geophys. Res. Lett.*, *3*, 727-730, doi:10.1029/GL003i012p00727.
- England, S.L., G. Liu, P. Withers, E. Yiğit, D. Lo, S. Jain, N.M. Schneider, J. Deighan, W.E. McClintock, P.R. Mahaffy, M. Elrod, M. Benna, and B.M. Jakosky (2016), Simultaneous observations of atmospheric tides from combined in situ and remote observations at Mars from the MAVEN spacecraft, *J. Geophys. Res. Planets*, *121*, doi:10.1002/2016JE004997.
- Forget, F., F. Montemessin, J.-L. Bertaux, F. González-Galindo, S. Lebonnois, E. Quémerais, A. Reberac, E. Dimarells, and M.A. López-Valverde (2009), Density and temperatures of the upper Martian atmosphere measured by stellar occultations with Mars Express SPICAM, *J. Geophys. Res.*, *114*, E01004, doi:10.1029/2008JE003086.
- Forbes, J.M., and M.E. Hagan (2000), Diurnal Kelvin wave in the atmosphere of Mars: Towards an understanding of “stationary” density structures observed by the MGS accelerometer, *Geophys. Res. Lett.*, *27*(21), 3563-3566, doi:10.1029/2000GL011850.
- Forbes, J.M., A.F.C. Bridger, S.W. Bougher, M.E. Hagan, J.L. Hollingsworth, G.M. Keating, and J. Murphy (2002), Nonmigrating tides in the thermosphere of Mars, *J. Geophys. Res.*, *107*(E11), 5113, doi:10.1029/2001JE001582.
- Forbes, J.M. and S. Miyahara (2006), Solar semidiurnal tide in the dusty atmosphere of Mars, *J. Atmos. Sci.*, *63*, 1798-1817, doi:10.1175/JAS3718.1.
- Hinson, D.P., R.A. Simpson, J.D. Twicken, G.L. Tyler, and F.M. Flasar (1999), Initial results from radio occultation measurements with Mars Global Surveyor, *J. Geophys. Res.*, *104*, 26,997-27,012.

- Jakosky, B.M., et al. (2015), The Mars Atmosphere and Volatile Evolution (MAVEN) Mission, *Space Sci. Rev.*, doi:10.1007/s11214-015-0139-x.
- Keating, G.M., S.W. Bougher, R.W. Zurek, R.H. Tolson, G.J. Cancro, S.N. Noll, J.S. Parker, T.J. Schellenberg, R.W. Shane, B.L. Wilerson, J.R. Murphy, J.L. Hollingsworth, R.M. Haberle, M. Joshi, J.C. Pearl, B.J. Conrath, M.D. Smith, R.T. Clancy, R.C. Blanchard, R.G. Wilmoth, D.F. Rault, T.Z. Martin, D.T. Lyons, P.B. Esposito, M.D. Johnston, C.W. Whetzel, C.G. Justus, J.M. Babicke (1998), The structure of the upper atmosphere of Mars: In situ accelerometer measurements from Mars Global Surveyor, *Science*, 279, 1672-1676.
- Korablev, O. I., J.-L. Bertaux, and J.-P. Dubois (2001), Occultation of stars in the UV: Study of the atmosphere of Mars, *J. Geophys. Res.*, 106, 7597-7610.
- Lee, C., et al. (2009), Thermal tides in the Martian middle atmosphere as seen by the Mars Climate Sounder, *J. Geophys. Res.*, 114, E03005, doi:10.1029/2008JE003285.
- Lo, D.Y., et al. (2015), Non-migrating tides in the Martian atmosphere as observed by MAVEN IUVS, *Geophys. Res. Lett.*, 42, 9057-9063, doi:10.1002/2015GL066268.
- Mahaffy, P.R., et al. (2014), The neutral gas and ion mass spectrometer on the Mars Atmosphere and Volatile Evolution Mission, *Space Sci. Rev.*, 185, doi:10.1007/s11214-11014-10091-11211.
- Mahaffy, P.R., M. Benna, M. Elrod, R.V. Yelle, S.W. Bougher, S.W. Stone, and B.M. Jakosky (2015), Structure and composition of the neutral upper atmosphere of Mars from the MAVEN NGIMS investigation, *Geophys. Res. Lett.*, 42, 8951-8957, doi:10.1002/2015GL065329.
- Mazarico, E., M.T. Zuber, F.G. Lemoine, and D.E. Smith (2008), Observations of atmospheric tides in the Martian exosphere using Mars Reconnaissance Orbiter radio tracking data, *Geophys. Res. Lett.*, 35, L09202, doi:10.1029/2008GL033388.
- McClintock, W.E., N.M. Schneider, G.M. Holsclaw, J.T. Clarke, A.C. Hoskins, I. Stewart, F. Montmessin, R.V. Yelle, and J. Deighan (2014), The Imaging Ultraviolet Spectrograph (IUVS) for the MAVEN Mission, *Space Sci. Rev.*, doi:10.1007/s11214-014-0098-7.
- Moudden, Y., and J.M. Forbes (2008), Topographic connection with density waves in Mars' aerobraking regime, *J. Geophys. Res.*, 113, E11009, doi:10.1029/2008JE003107.
- Moudden, Y., and J.M. Forbes (2014), Insight into the seasonal asymmetry of nonmigrating tides on Mars, *Geophys. Res. Lett.*, 41, 2631-2636, doi:10.1002/2014GL059535.
- Oberheide, J., and J.M. Forbes (2008), Thermospheric nitric oxide variability induced by nonmigrating tides, *Geophys. Res. Lett.*, 35, L16814, doi:10.1029/2008GL034825.

- Seth, S.P., U.B. Jayanthi, and S.A. Haider (2006), Estimation of peak electron density in upper ionosphere of Mars at high latitude ( $50^{\circ}$ - $70^{\circ}$ ) using MGS ACC data, *Geophys. Res. Lett.*, *33*, L19204, doi:10.1029/2006GL027064.
- Snowden, D., R.V. Yelle, J. Cui, J.-E. Wahlund, N.J.T. Edberg, K. Ågren (2013), The thermal structure of Titan's upper atmosphere, I: Temperature profiles from Cassini INMS observations, *Icarus*, *226*, 552-582.
- Tolson, R.H., A.M., Dwyer, J.L. Hanna, G.M. Keating, B.E. George, P.E. Escalera, and M.R. Werner (2005), Application of accelerometer data to Mars Odyssey aerobraking and atmospheric modeling, *J. Spacecr. Rockets*, *42*, 435-443.
- Tolson, R.H., E. Bermis, S. Hough, K. Zaleski, G. Keating, J. Shidner, S. Brown, A. Brickler, M. Scher, and P. Thomas (2008), Atmospheric modeling using accelerometer data during Mars Reconnaissance Orbiter aerobraking operations, *J. Spacecr. Rocket.*, *45*, 511-518.
- Wilson, R.J. (2002), Evidence for nonmigrating thermal tides in the Mars upper atmosphere from the Mars Global Surveyor accelerometer experiment, *Geophys. Res. Lett.*, *29* (7), 1120, doi:10.1029/2001GL013975.
- Withers, P., S.W. Bougher, and G.M. Keating (2003), The effects of topographically-controlled thermal tides in the Martian upper atmosphere as seen by the MGS accelerometer, *Icarus*, *164*, 14-32, doi:10.1016/S0019-1035(03)00135-0.
- Withers, P. (2006), Mars Global Surveyor and Mars Odyssey accelerometer observations of the martian upper atmosphere during aerobraking, *Geophys. Res. Lett.*, *33*, L02201, doi:10.1029/2005GL024447.
- Withers, P., R. Pratt, J.-L. Bertaux, and F. Montmessin (2011), Observations of thermal tides in the middle atmosphere of Mars by the SPICAM instrument, *J. Geophys. Res.*, *116*, doi:10.1029/2011JE003847.
- Yigit, E., S.L. England, G. Liu, A.S. Medvedev, P.R. Mahaffy, T. Kuroda, and B.M. Jakosky (2015), High-altitude gravity waves in the Martian thermosphere observed by MAVEN/NGIMS and modeled by a gravity wave scheme, *Geophys. Res. Lett.*, *42*, doi:10.1002/2015GL065307.